Fluctuation broadening in carbon nanotube resonators

Arthur W. Barnard[a], Vera Sazonova[b], Arend M. van der Zande[b], and Paul L. McEuen[b,c,1]

[a]Applied and Engineering Physics, [b]Laboratory of Atomic and Solid State Physics, and [c]Kavli Institute at Cornell for Nanoscale Science, Cornell University, Ithaca, NY 14853

Contributed by Paul L. McEuen, October 5, 2012 (sent for review April 18, 2012)

We simulated the behavior of suspended carbon nanotube resonators over a broad range of temperatures to explore the physics of semiflexible polymers in underdamped environments. We find that thermal fluctuations induce strong coupling between resonance modes. This effect leads to spectral fluctuations that readily account for the experimentally observed quality factors $Q \sim 100$ at 300 K. Using a mean-field approach to describe fluctuations, we analytically calculate Q and frequency shifts in tensioned and buckled carbon nanotubes and find excellent agreement with simulations.

nanomechanics | stochastic dynamics | nonlinear vibrations | mesoscopic physics

The effects of thermal fluctuations can completely alter the mechanical properties of reduced dimensional systems. For example, the shape and elasticity of a DNA molecule are entirely dominated by thermal fluctuations of transverse degrees of freedom, completely altering both physical behavior and biological function. In overdamped environments such as liquids, these entropic effects have been studied for decades (1), but the behavior of reduced elastic objects in underdamped environments is largely unexplored. For example, consider a resonator made from an atomically thin membrane or polymer. How will thermal fluctuations affect the vibrational spectrum, and how will thermally driven nonlinear effects influence the decay widths of the resonance modes?

Carbon nanotube (CNT) resonators, with their nanometer-scale cross-section (2) and very small bending rigidity for flexural modes (3) present a unique opportunity to probe these questions. Experimental work has shown CNT resonators to be highly tunable (4) as well as functional as rf transceivers (5) and atomic mass detectors (6, 7), but these resonators have consistently exhibited much broader than expected decay widths (4, 8). Specifically, the quality factor Q, the key parameter measuring the degree to which an oscillating mode is decoupled from its environment, which is inferred from the decay width, is typically less than $Q \sim 100$ at room temperature. These low Qs are not consistent with known dissipation mechanisms seen in other nanomechanical resonator systems (9). Analytical phonon-phonon scattering studies establish a theoretical upper bound on Q in CNTs that is well above experimental values, with $Q \lesssim 50{,}000$ at 300 K (10, 11). Molecular-dynamics simulations of short CNTs ($L \sim 50$ nm) show interesting behaviors in cantilevered and free CNT segments (12–15) due to anharmonic atomic potentials, and those that make an explicit determination of quality factor in thermal equilibrium (13, 14) give $Q \sim 1{,}000$ at room temperature. Typically, however, experiments are performed on CNTs with $L \gtrsim 1$ μm, and the anharmonic elastic effects that dominate in short-length CNTs do not contribute as significantly at this longer length scale.

An alternative explanation for these altered properties comes from the field of polymer physics, where the effects of fluctuations on the physics of 1D elastic objects have a long and storied history. A key length-scale that characterizes these 1D objects' properties is the persistence length $\ell_p = \frac{\kappa}{k_B T}$, where κ is the bending rigidity. Subject to thermal forces, the 1D elastic object will fluctuate and lose correlations in shape for lengths longer than ℓ_p. Thus, short 1D structures ($L \ll \ell_p$) such as microfabricated nanobeam resonators behave like rigid rods, with thermal amplitudes small compared with the size of the structure. However, long 1D structures ($L \gg \ell_p$) such as organic polymers are forced into fluctuating, coiled, high-entropy configurations. Micron-scale CNTs are between these regimes, in the semiflexible polymer limit ($L \lesssim \ell_p$) (1), where the bending energy and configurational entropy contribute comparably to the total free energy. In overdamped environments, the behavior of semiflexible polymers is now well understood (16), but the behavior of a nanoscale resonator in the semiflexible polymer limit has not been explored.

In this article, we report simulations and analytical predictions of the thermally driven dynamics of CNT resonators over temperatures from 3 to 300 K and in the limits of both compressive and tensile strain. By simulating purely continuum elastic behavior, we isolate the specific influence of entropic forces on measured quantities, including both quality factor and thermally induced frequency shifts. Quantum mechanical effects are neglected, because the thermal occupation of all modes considered are in the classical limit. We find that the fluctuations of many resonance modes strongly influence the quality factor of CNT resonators, an effect called fluctuation broadening, which was previously invoked in the context of molecular spectra (17). We find that this fluctuation broadening is in good agreement with observed quality factors in experiment.

CNTs were modeled as 1D linear-elastic objects, with bending rigidity $\kappa = \pi\frac{Cd^3}{8}$ and extensional rigidity $K = \pi Cd$, where $C \sim 345$ J/m^2 (18) is the 2D elastic modulus of graphene and d is the tube diameter. Each CNT was discretized into 100 or more masses joined by axial and torsional linear springs. For a given set of tube dimensions, boundary conditions, and externally applied forces, the equilibrium geometry was computed via a relaxation method, and zero-temperature eigenmodes were computed by diagonalizing the force constant matrix (19) (details in *SI Text*).

Results

To study dynamics at nonzero temperature, a finite time-difference calculation was used. Thermal equilibrium was reached by coupling the nanotube to an external heat-bath via a generalized Langevin equation, applying a stochastic white-noise force with external damping. Dynamics at equilibrium were then simulated with this Langevin equation using the fourth-order Runge–Kutta method. Adiabatic conditions were also studied using Stoermer's rule (20). The model's validity was confirmed by its ability to properly exhibit equipartition of energies for each eigenmode. Additionally, we performed externally driven simulations and found similar Q at low amplitude drive compared with the thermally driven simulation data we present.

Throughout this article, data are shown from simulations of a typical experimental case of a CNT with $L = 3$ μm and $d = 2$ nm. We investigate resonance properties of this CNT at different zero-temperature strains ϵ_0, temperatures T, and externally

Author contributions: A.W.B., V.S., A.M.v.d.Z., and P.L.M. designed research; A.W.B. performed research; A.W.B., V.S., A.M.v.d.Z., and P.L.M. analyzed data; and A.W.B. and P.L.M. wrote the paper.

The authors declare no conflict of interest.

[1]To whom correspondence should be addressed. E-mail: plm23@cornell.edu.

This article contains supporting information online at www.pnas.org/lookup/suppl/doi:10.1073/pnas.1216407109/-/DCSupplemental.

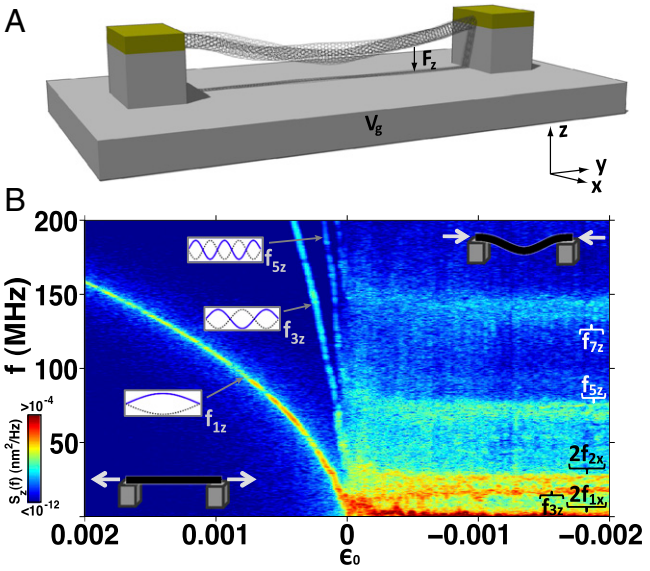

Fig. 1. (*A*) Schematic of CNT resonator geometry. CNT is suspended between two electrodes (in yellow) and has a controllable downward force F_z electrostatically applied by a voltage to the underlying substrate. A small F_z is applied in *B* to keep the buckled tube oriented vertically. (*B*) Simulated power spectral density of the *z*-motion of the nanotube as a function of strain ϵ_0 at $T = 100$ *K* with logarithmic color scale. The tube is taken from tensile strain (*Left*) to compressive strain (*Right*) as illustrated (*Insets*). Eigenmode shapes are inset, as are labels for the eigenfrequencies.

applied forces F_z by quasi-statically sweeping at most one parameter and measuring the power spectral density of the mean *z*-displacement (defined in Fig. 1*A*) of the nanotube: $S_z(f) = \lim_{t_m\to\infty} E\left[\frac{|\mathcal{F}(z_{t_m}(t))|^2}{t_m}\right]$, where t_m is the finite time over which the Fourier transform is taken, and E denotes an ensemble average. The mean *z*-displacement was the chosen parameter to analyze because it is typically measured in experiments (21). From $S_z(f)$, we measure thermal frequency shifts $\Delta f \equiv f - f(T = 0\ K)$ and quality factor $Q \equiv \frac{f}{\delta f}$. This definition of Q is used because the linewidth δf is directly measured in experiments.

We first study the qualitative behavior of this CNT as a function of strain at 100 *K*. In the tensioned limit (Fig. 1*B*, *Left*), the eigenmodes, labeled by their modeshape, tune like a tensioned string, giving a frequency $f_n \approx \frac{n}{2L}\sqrt{\frac{N}{\mu}}$, where μ is the linear mass density and $n = K\epsilon$ is the axial tension. Modes without mean *z*-displacements, including the even in-plane (*z*-direction) eigenmodes and all out-of-plane (*x*-direction) eigenmodes, are not visible. Thus, only modes with $n = 1, 3, 5\ldots$ are seen.

With negative strain, the nanotube undergoes a Euler buckling transition, as illustrated in Fig. 1*B Upper Right*. With the resulting built-in slack, the CNT can bend without stretching, leading the spectral lines to no longer tune significantly with strain. The linewidths, however, do tune with strain (Fig. S1). Also, there are emergent spectral lines corresponding to the motion of out-of-plane modes (Fig. 1*B*, *Right*). We analyze these temperature-dependent linewidths in the tensioned case and buckled case separately and discuss the different nonlinear coupling mechanisms (22–24) that apply to each.

Tensioned Nanotube. We begin with the tensioned case. We select a fixed tensile zero-temperature clamping condition $\epsilon_0 = 2 \times 10^{-4}$, and simulate the nanotube motion at six temperatures, incrementing by 50 *K* from 50 to 300 *K* and plot in Fig. 2*A* the power spectral density over a frequency range spanning up to the $n = 5$ mode. The frequencies of the modes shift linearly with T and, as shown in Fig. 2*C*, the peaks also broaden with $Q^{-1} \sim T$. At 300 *K*, $Q \sim 40$. The quality factor and frequency shifts can be understood to arise from the change in length of the CNT caused by thermal fluctuation in each eigenmode. The n^{th} eigenmode is given by $u_{na}(y,t) = a_n(t)\xi_{na}\left(\frac{y}{L}\right)$, where ξ_{na} is the dimensionless modeshape with unit rms displacement, a_n is a time-varying amplitude function, and both the amplitude a and index a refer to either the x or y direction. The tube elongates by the length $\beta_{na}\frac{a_n^2}{2L}$, where $\beta_{na} \equiv \int_0^1 \xi'_{na}(x)^2 dx$ for each independent eigenmode; this leads to the strain being modified as $\langle\epsilon\rangle \approx \epsilon_0 + \sum_{n,a}\beta_{na}\frac{\langle a_n^2\rangle}{2L^2}$, where brackets denote a time average over the period of oscillation (25). Assuming that $\langle a_n\rangle$ obey Boltzmann statistics in thermal equilibrium and that a_n fluctuate incoherently, we are able to solve for the mean strain shift $\overline{\Delta\epsilon}$ and strain variance σ_ϵ^2 (details in *SI Text*).

In the high-tension limit, a large number of the resonance modes contribute significantly to length fluctuations. Accounting for the contribution of all resonance modes gives for the mean-field strain shift

$$\overline{\Delta\epsilon} = \frac{L}{2n_f\ell_p}; \quad n_f = \sqrt{\frac{NL^2}{\kappa}}, \qquad [1]$$

where the value of $\overline{\Delta\epsilon}$ is solved self-consistently, and n_f can be interpreted as the number of independent degrees of freedom causing significant length fluctuations. Here, high-frequency modes do not appreciably modify the strain, because most of their elastic energy is stored in bending rather than in stretching. $\overline{\Delta\epsilon}$ is a length-dependent thermal expansion parameter that is distinct from the intrinsic thermal expansion simulated for CNTs (12). From Eq. **1**, $\overline{\Delta\epsilon}$ leads to $\Delta f \sim T$.

Next, we calculate the strain variance $\sigma_\epsilon^2 = \frac{L^2}{8n_f^3\ell_p^2}$, which leads to the prediction that $\delta f \sim T$. Furthermore, the predicted δf constitutes fluctuation broadening and gives a unique prediction for Q (derivation in *SI Text*):

$$Q^{-1} = \frac{\sqrt{\ln 2}}{2}\frac{L}{n_f^{\frac{3}{2}}\epsilon\ell_p}. \qquad [2]$$

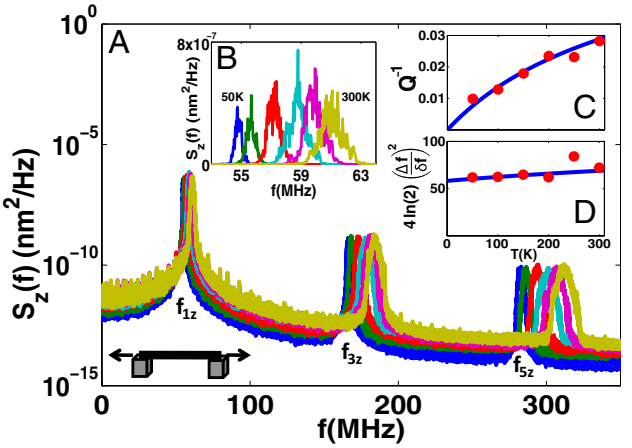

Fig. 2. (*A*) Power spectral density of a tensioned nanotube with $\epsilon_0 = 2 \times 10^{-4}$. Six temperatures are plotted from 50 to 300 *K* spaced evenly in *T*. (*B*) Linear plot of S_z (*f*) for f_{1z} showing that the frequency shift Δf and line width δf both scale linearly with *T*. (*C*) Inverse quality factor of f_{1z} vs. temperature. (*D*) Dimensionless fixed ratio of Δf to δf that corresponds to n_f, the number of independent fluctuating modes contributing to spectral broadening and frequency shifts. In *C* and *D*, data are circles, and theory is a line. The line in *C* corresponds to Eq. **2**, and in *D* n_f in Eq. **1**.

Eq. **2** is our first key result. The dominant T-dependence comes from $\ell_p^{-1} \sim T$, but both n_f and ϵ have weak T-dependence as a result of entropic stretching. The quantity $n_f^2 \ell_p$ is the persistence length for a tensioned beam and parameterizes how far fluctuations drive the CNT out of equilibrium. The $n_f^{\frac{3}{2}}$ dependence then can be understood to arise from an additional linewidth broadening $\sim n_f^{\frac{1}{2}}$ due to averaging over n_f uncorrelated degrees of freedom. Eq. **2** accurately describes the numerical results, shown in Fig. 2*C*, and shows that fluctuation broadening can account for the experimentally observed $Q \sim 100$ at room temperature (8, 21).

Buckled Nanotube. Next, we study a nanotube under compressive strain, picking $\epsilon_0 = -4 \times 10^{-3}$. Applying a small downward force $F_z = 0.6\ pN$ that mimics the force applied by the gate in experiments, simulations were performed at logarithmically spaced temperatures from 3.1 to 300 K, as shown in Fig. 3. In contrast to the tensioned regime, there is complex structure in the spectra, with many spectral features growing nonlinearly with T. Linear theory predicts that f_{3z} and f_{5z} would be the only visible spectral lines in Fig. 3. The other emergent modes can be identified as either oscillations of out-of-plane modes producing z-displacement at twice their natural frequency ($2f_{1x}$, $2f_{2x}$, and $2f_{3x}$) or mixes of in-plane modes ($f_{5z} - f_{3z}$ and $f_{5z} + f_{3z}$). Focusing on the lowest observed in-plane mode (f_{3z}), we observe $Q^{-1} \sim T$ (Fig. 3, *Inset*) and a decrease in frequency with increasing temperature. From this we extract $Q \sim 5$ for this mode at 300 K.

Further insight is gained by smoothly tuning frequencies by quasi-statically varying the magnitude of the electrostatic force $F_z = \frac{1}{2} C' V_g^2$, as shown in Fig. 4 *A* and *B*, where V_g corresponds to the electrostatic voltage applied to the gate illustrated in Fig. 1*A*, and $C' = \frac{dC}{dz}$ is the derivative of the tube-gate capacitance assuming a 400-nm gap. The spectral lines tune with force and the frequency-doubled out-of-plane spectral lines cut across the in-plane spectral lines. At 0 K, linear theory predicts there to be no coupling. However, at the intersections, there are observable avoided crossings, even at 10 K, as seen in Fig. 4*A*. This behavior is consistent with experiments (21). To study this, we fix F_z at a crossing indicated by the dotted line in Fig. 4*A*, quasi-statically sweep the temperature, and measure $S_z(f)$ (Fig. 4*A*, *Inset*). Here, we observe a sublinear T-dependence of the splitting at the avoided crossing. At 300 K, the frequency splitting is nearly one-fifth of the resonance frequency, indicating a strong coupling strength induced entirely by thermal fluctuations.

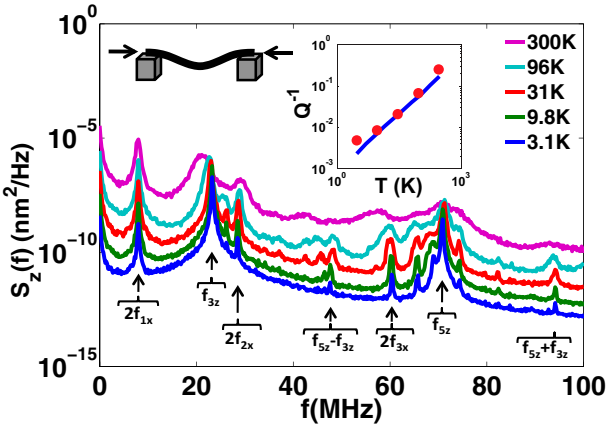

Fig. 3. Power spectral density of buckled nanotube with $\epsilon_0 = -4 \times 10^{-3}$ with $F_z = 0.6\ pN$ at logarithmically spaced temperatures. The built-in intrinsic damping dominates the apparent line width at the lowest temperature. (*Inset*) Plot of Q^{-1} of the f_{3z} mode. Simulation data are shown as red dots, and theoretical predictions from Eq. **3** are plotted as a blue line. Labels beneath each spectral line correspond to their expected origin.

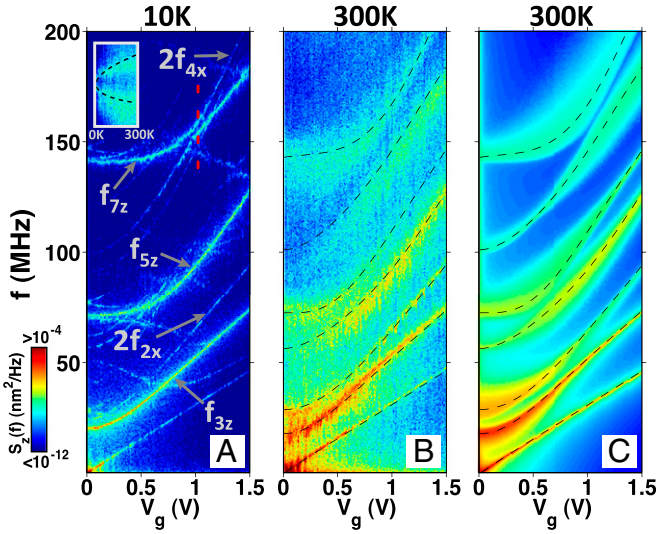

Fig. 4. (*A*) Color map of power spectral density at 10 K of the mean z-displacement of a buckled nanotube resonator as a function of gate voltage, assuming tube is 400 nm above the gate. Modes are labeled as defined in Fig. 3, and color scale is identical to that in Fig. 1*B*. T-dependence from 0 to 300 K of the apparent avoided-crossing at 150 MHz is shown (*Inset*) at a fixed V_g indicated by the red dotted line. (*B*) 300 K data of same force sweep in *A*. (*C*) Plot of the theoretical power spectral density, based on the generalized version of Eq. **3** described in the text, for the same conditions as in *B*. The dashed lines in *B* and *C* correspond to the theoretical central frequencies from the generalized version of Eq. **3**.

We build an analytical model for this behavior by first modeling the CNT as an inextensible object. In this framework, when an out-of-plane mode has finite amplitude, the CNT must move up in the z-direction to preserve length. To quantify the amount that the tube moves in z, we enforce the constraint that the differential length $dL = \sqrt{\beta_{1z}|\epsilon|}dz_1 - 2\sum_n \frac{\beta_{1x} x_n}{L} dx_n$ is zero, where the equilibrium deflection of the tube is $z_1 \xi_{1z}\left(\frac{y}{L}\right)$. ξ_{1z} is a linear combination of in-plane modes, requiring to second order that $z_{nNL} = z_n + \frac{\eta_n}{L}\sum_m \beta_{mx} x_m^2$, where $\eta_n \equiv \frac{\langle \xi_{1z} | \xi_{nz} \rangle}{\langle \xi_{nz} | \xi_{nz} \rangle} \frac{2}{\sqrt{\beta_{1z}|\epsilon|}}$, in which the brackets are an inner product defined by $\langle a(x)|b(x)\rangle = \int_0^1 a(x)b(x)dx$ (25).

Focusing on the interaction of one in-plane and one out-of-plane mode, we change the out-of-plane variable to $z_{op} = \frac{\eta}{L}\beta_{op} x_{op}^2$ and apply time-dependent perturbation theory (26) (details in *SI Text*) to generate a coupled set of linearized equations:

$$\begin{bmatrix} -k_{ip} & \alpha(T)k_{ip} \\ \alpha(T)k_{ip} & -4k_{op} - \frac{3}{2}\alpha^2(T)k_{ip} \end{bmatrix} \begin{bmatrix} z_{ip} \\ z_{op} \end{bmatrix} = m \begin{bmatrix} \ddot{z}_{ip} \\ \ddot{z}_{op} \end{bmatrix}, \qquad [3]$$

where $\alpha(T) \equiv \frac{4\eta\beta_{op}\sqrt{\langle x_{op}^2 \rangle}}{L}$ and $\langle x_{op}^2 \rangle$ is time-averaged over the period of oscillation.

Using $\langle x_{op}^2 \rangle = \frac{k_B T}{k_{op}}$ gives $\alpha(T) \sim \sqrt{T}$, which when substituted into Eq. **3** predicts average frequency shifts. At an avoided crossing, $k_{ip} \sim 4k_{op}$ gives the prediction that $\Delta f \approx \frac{1}{2}\alpha(T) f_{ip}$; this matches the simulated T-dependence, as shown by the theoretical prediction that is overlaid on top of the data in Fig. 4*A* *Inset*.

By extending Eq. **3** to the full interaction matrix, populating each mode according to Boltzmann statistics, and weighting the resulting frequency probability distribution by the squared-amplitude distribution, we are able to generate a theoretical $S_z(f)$ map, which is shown in Fig. 4*C*; it compares well with the

simulated results at 300 K shown in Fig. 4B. In addition, the linewidths in the theoretical S_z (f) give an accurate prediction of the simulated Qs, as shown in Fig. 3 *Inset*. The specific degree of coupling is geometry-dependent, and thus not fully analytically generalizable, but Eq. **3** predicts for the lowest in-plane mode f_{3z} that

$$Q^{-1} \approx 0.04 \frac{L}{|\epsilon|\ell_p}. \quad [4]$$

Eq. **4** (derivation shown in *SI Text*) explains the strain dependence of the spectral fluctuations seen in Fig. 1A *Right*: Q improves with increased buckling as the geometric coupling between modes decreases. Furthermore, due to its coupling with higher-frequency modes, the lowest in-plane mode is predicted to decrease frequency with increasing temperature at low V_g, which is frequently observed in experiment (7, 21).

Discussion

These results show that fluctuation broadening dominates the behavior of CNT resonators over a broad range of temperatures, and appears to be the main cause of temperature-dependent quality factors measured in both tensioned and untensioned resonators. Understanding the mechanism behind fluctuation broadening in CNT resonators draws on the ideas of polymer physics and underscores how thermal fluctuations can strongly modify the vibrational spectrum and decay widths in reduced dimensional nanoscale objects. To date there is limited experimental data characterizing Q over a broad temperature range in CNT resonators, but thus far, data remain at or below our theoretical upper bound (8, 21, 27). We predict a specific dependence of Q on ϵ_0 and T that can be tested by experiments that vary these parameters independently on individual CNT resonators. Specifically, varying ϵ_0 at a fixed T will be the most informative for this work, because the interpretation will be less obscured by systematic strain shifts that occur due to thermal expansion of the system.

This work implies a fundamental limit on Q in high aspect-ratio resonators at finite temperatures. Tailoring the geometry of these systems is necessary to mitigate thermally induced mode-coupling and thus improve Q.

ACKNOWLEDGMENTS. This work was supported by National Science Foundation (NSF) Grant 0928552 and the Cornell Center for Materials Research (CCMR) with funding from Integrative Graduate Education and Research Traineeship in Nanoscale Control of Surfaces and Interfaces DGE-0654193. We made use of the research computing facility of the CCMR with support from the National Science Foundation Materials Research Science and Engineering Centers Program DMR-0520404.

1. Fakhri N, Tsyboulski DA, Cognet L, Weisman RB, Pasquali M (2009) Diameter-dependent bending dynamics of single-walled carbon nanotubes in liquids. *Proc Natl Acad Sci USA* 106(34):14219–14223.
2. Postma HWC, Kozinsky I, Husain A, Roukes ML (2005) Dynamic range of nanotube- and nanowire-based electromechanical systems. *Appl Phys Lett* 86(22):3105–3107.
3. Verbridge SS, Parpia JM, Reichenbach RB, Bellan LM, Craighead HG (2006) High quality factor resonance at room temperature with nanostrings under high tensile stress. *J Appl Phys* 99(12):4304–4311.
4. Sazonova V, et al. (2004) A tunable carbon nanotube electromechanical oscillator. *Nature* 431(7006):284–287.
5. Jensen K, Weldon J, Garcia H, Zettl A (2007) Nanotube radio. *Nano Lett* 7(11): 3508–3511.
6. Jensen K, Kim K, Zettl A (2008) An atomic-resolution nanomechanical mass sensor. *Nat Nanotechnol* 3(9):533–537.
7. Lassagne B, Garcia-Sanchez D, Aguasca A, Bachtold A (2008) Ultrasensitive mass sensing with a nanotube electromechanical resonator. *Nano Lett* 8(11):3735–3738.
8. Eichler A, et al. (2011) Nonlinear damping in mechanical resonators made from carbon nanotubes and graphene. *Nat Nanotechnol* 6(6):339–342.
9. Cleland AN, Roukes ML (2002) Noise processes in nanomechanical resonators. *J Appl Phys* 92(5):2758–2769.
10. Hepplestone SP, Srivastava GP (2006) Phonon-phonon interactions in single-wall carbon nanotubes. *Phys Rev B* 74(16):5420.
11. Lischner J, Arias TA (2010) Material limitations of carbon-nanotube inertial balances: Possibility of intrinsic yoctogram mass resolution at room temperature. *Phys Rev B* 81(23):3409.
12. Kwon YK, Berber S, Tománek D (2004) Thermal contraction of carbon fullerenes and nanotubes. *Phys Rev Lett* 92(1):015901.
13. Feng EH, Jones RE (2010) Equilibrium thermal vibrations of carbon nanotubes. *Phys Rev B* 81(12):5436.
14. Jiang H, Yu MF, Liu B, Huang Y (2004) Intrinsic energy loss mechanisms in a cantilevered carbon nanotube beam oscillator. *Phys Rev Lett* 93(18):185501.
15. Greaney PA, Lani G, Cicero G, Grossman JC (2009) Anomalous dissipation in single-walled carbon nanotube resonators. *Nano Lett* 9(11):3699–3703.
16. Wiggins PA, Nelson PC (2006) Generalized theory of semiflexible polymers. *Phys Rev E Stat Nonlin Soft Matter Phys* 73(3 Pt 1):031906.
17. Dykman MI, McClintock PVE (1992) Power spectra of noise-driven nonlinear systems and stochastic resonance. *Physica D* 58(1-4):10–30.
18. Kudin KN, Scuseria GE, Yakobson BI (2001) C(2)F, BN, and C nanoshell elasticity from ab initio computations. *Phys Rev B* 64(23):5406.
19. Ustünel H, Roundy D, Arias TA (2005) Modeling a suspended nanotube oscillator. *Nano Lett* 5(3):523–526.
20. Press WH, Teukolsky SA, Vetterling WT, Flannery BP (1992) *Numerical Recipes in C* (Cambridge Univ Press, Cambridge), 2nd Ed, pp 707–747.
21. Sazonova VA (2006) *A tunable carbon nanotube resonator*. PhD dissertation (Cornell University, Ithaca, NY).
22. Nayfeh AH, Mook DT, Sridhar S (1974) Nonlinear analysis of the forced response of structural elements. *J Acoust Soc Am* 55(2):281–291.
23. Conley WG, Raman A, Krousgrill CM, Mohammadi S (2008) Nonlinear and nonplanar dynamics of suspended nanotube and nanowire resonators. *Nano Lett* 8(6): 1590–1595.
24. Dykman MI, Krivogla MA (1971) Classical theory of nonlinear oscillators interacting with a medium. *Phys Status Solidi B* 48(2):497–512.
25. Westra HJR, Poot M, van der Zant HSJ, Venstra WJ (2010) Nonlinear modal interactions in clamped-clamped mechanical resonators. *Phys Rev Lett* 105(11):117205.
26. Nayfeh AH, Mook DT (2007) *Nonlinear Oscillations* (Wiley, New York), pp 444–507.
27. Hüttel AK, et al. (2009) Carbon nanotubes as ultrahigh quality factor mechanical resonators. *Nano Lett* 9(7):2547–2552.